The Journal of Immunology

This information is current as of February 24, 2022.

Tolerogenic versus Immunogenic Lipidomic Profiles of CD11c $^{+}$ Immune Cells and Control of Immunogenic Dendritic Cell Ceramide Dynamics

Carlos Ocaña-Morgner, Susanne Sales, Manuela Rothe, Andrej Shevchenko and Rolf Jessberger

J Immunol 2017; 198:4360-4372; Prepublished online 3 May 2017;
doi: 10.4049/jimmunol.1601928
http://www.jimmunol.org/content/198/11/4360

Supplementary Material **http://www.jimmunol.org/content/suppl/2017/05/03/jimmunol.1601928.DCSupplemental**

References This article **cites 68 articles**, 31 of which you can access for free at:
http://www.jimmunol.org/content/198/11/4360.full#ref-list-1

Why *The JI*? Submit online.

- **Rapid Reviews! 30 days*** from submission to initial decision
- **No Triage!** Every submission reviewed by practicing scientists
- **Fast Publication!** 4 weeks from acceptance to publication

**average*

Subscription Information about subscribing to *The Journal of Immunology* is online at:
http://jimmunol.org/subscription

Permissions Submit copyright permission requests at:
http://www.aai.org/About/Publications/JI/copyright.html

Email Alerts Receive free email-alerts when new articles cite this article. Sign up at:
http://jimmunol.org/alerts

The Journal of Immunology is published twice each month by
The American Association of Immunologists, Inc.,
1451 Rockville Pike, Suite 650, Rockville, MD 20852
Copyright © 2017 by The American Association of Immunologists, Inc. All rights reserved.
Print ISSN: 0022-1767 Online ISSN: 1550-6606.

Downloaded from http://www.jimmunol.org/ by guest on February 24, 2022

Tolerogenic versus Immunogenic Lipidomic Profiles of CD11c$^+$ Immune Cells and Control of Immunogenic Dendritic Cell Ceramide Dynamics

Carlos Ocaña-Morgner,* Susanne Sales,† Manuela Rothe,* Andrej Shevchenko,† and Rolf Jessberger*

Lipids affect the membrane properties determining essential biological processes. Earlier studies have suggested a role of switch-activated protein 70 (SWAP-70) in lipid raft formation of dendritic cells. We used lipidomics combined with genetic and biochemical assays to analyze the role of SWAP-70 in lipid dynamics. TLR activation using LPS as a ligand represented a pathogenic immunogenic stimulus, physical disruption of cell–cell contacts a tolerogenic stimulus. Physical disruption, but not LPS, caused an increase of phosphatidylcholine ether and cholesteryl esters in CD11c$^+$ immune cells. An increase of ceramide (Cer) was a hallmark for LPS activation. SWAP-70 was required for regulating the increase and localization of Cers in the cell membrane. SWAP-70 controls Cer accumulation through the regulation of pH-dependent acid-sphingomyelinase activity and of RhoA-dependent transport of endosomal contents to the plasma membrane. Poor accumulation of Cers in *Swap70*$^{-/-}$ cells caused decreased apoptosis. This shows that two different pathways of activation, immunogenic and tolerogenic, induce different changes in the lipid composition of cultured CD11c$^+$ cells, and highlights the important role of SWAP-70 in Cer dynamics in dendritic cells. ***The Journal of Immunology*****, 2017, 198: 4360–4372.**

Dendritic cells (DCs) are potent APCs that initiate cellular immune responses by activating CD4$^+$ and CD8$^+$ T cells (1). After encounter with microbes and/or inflammatory molecules in the skin and organs, DCs start a maturation process characterized by the migration to lymph nodes, Ag presentation, expression of costimulatory molecules, and secretion of inflammatory cytokines (1). The use of culture conditions that include GM-CSF has allowed the analysis of many aspects of DC biology in vitro (2, 3). In GM-CSF cultures, a CD11c$^+$ population develops, which contains DCs (CD11c$^+$CD86^{high}) that resemble the in vivo migratory DCs in mice (4). Dissociation of E-cadherin–dependent interactions between DCs by cluster disruption (CD) in these cultures is considered to induce a tolerogenic state, in contrast to the immunogenic state triggered by stimuli like bacterial LPS, a TLR ligand (5–7). Similar to the effects induced by some agents used to generate tolerogenic DCs, e.g., rapamycin and thymic stromal lymphopoietin (8, 9), mechanical disruption of cell–cell interactions led to upregulation of costimulatory molecules (CD83, CD86) and the CCR7 chemokine receptor in DCs of GM-CSF cultures, but failed to induce the production of inflammatory cytokines (6). Cluster-disrupted DCs also supported the expansion of a population of IL-10–producing regulatory CD4$^+$ T cells (6). However, CD differs from other tolerance-promoting agents like IL-10, dexamethasone, and 1α,25-dihydroxyvitamin D3 in that they, but not CD, induced downregulation of costimulatory molecules (8).

Switch-activated protein 70 (SWAP-70) is expressed in DCs and localizes in membrane areas at sites of cell–cell contact and of micropinosomes (10, 11). A pleckstrin homology domain exists in the center region of SWAP-70 that binds PIP3-mediating membrane localization of the protein (12). SWAP-70 also binds F-actin, but not G-actin, contributing to the rearrangement of the cytoskeleton by stabilizing F-actin (13, 14). SWAP-70 also loosely resembles proteins of the Dbl family of guanine nucleotide exchange factors for Rho GTPases (12). We demonstrated that SWAP-70 preferentially interacts with active RhoA (RhoA-GTP) and Rac1 (Rac1-GTP) in the lysates of stimulated DCs (10). Unlike wild-type (wt) DCs, naive *Swap70*$^{-/-}$ DCs show constitutively active RhoA (10). Important DC functions like localization of peptide-loaded MHC class II (MHCII), migration toward S1P, and spontaneous maturation are regulated through the control of RhoA activation by SWAP-70 (10, 15, 16).

In previous reports, we have demonstrated that *Swap70*$^{-/-}$ DCs fail to localize signaling proteins like the heterotrimeric Gα_{13} and MHCII to membrane rafts (10, 16). This evoked the speculation that through an unknown mechanism, SWAP-70 may contribute to the protein and/or lipid composition of lipid rafts and perhaps even to the total lipid composition of DCs. Lipids play essential biological roles as structural, signaling, and regulatory molecules in many cell processes. Local enrichment of certain lipids like cholesterol and ceramides (Cers) in raft structures in the plasma

*Institute of Physiological Chemistry, Faculty of Medicine Carl Gustav Carus, Dresden University of Technology, Dresden 01307, Germany; and †Max Planck Institute of Molecular Cell Biology and Genetics, Dresden 01307, Germany

ORCID: 0000-0003-3027-964X (C.O.-M.).

Received for publication November 11, 2016. Accepted for publication April 5, 2017.

This work was supported by Deutsche Forschungsgemeinschaft Grant OC 109/2-1 and by the Faculty of Medicine Carl Gustav Carus, Dresden.

Address correspondence and reprint requests to Dr. Carlos Ocaña-Morgner and Prof. Rolf Jessberger, Institut für Physiologische Chemie, Medizinische Fakultät Carl Gustav Carus, Technische Universität Dresden, Fiedlerstrasse 42, 01307 Dresden, Germany, Germany. E-mail addresses: carlos.ocana-morgner@mailbox.tu-dresden.de (C.O.-M.) and rolf.jessberger@mailbox.tu-dresden.de (R.J.)

The online version of this article contains supplemental material.

Abbreviations used in this article: BMDC, bone marrow–derived DC; CD, cluster disruption; CE, cholesteryl ester; Cer, ceramide; DAG, diacylglycerol; DC, dendritic cell; Flt3-L, Flt3 ligand; MFI, mean fluorescence intensity; MHCII, MHC class II; PAF, platelet-activating factor; PC-O, phosphatidylcholine ether; PG, phosphatidylglycerol; PI, phosphatidylinositol; SM, sphingomyelin; SWAP-70, switch-activated protein 70; TAG, triacylglycerol; wt, wild type.

Copyright © 2017 by The American Association of Immunologists, Inc. 0022-1767/17/$30.00

www.jimmunol.org/cgi/doi/10.4049/jimmunol.1601928

Downloaded from http://www.jimmunol.org/ by guest on February 24, 2022

membrane is known to facilitate segregation of membrane receptors and signalosome components, contributing to the signaling in a large variety of processes (17–19). Lipidomics has thus become a very important tool to study the presence and possibly function of different lipid classes in biological systems (20). In addition, the combination of lipidomic, biochemical, and genetic assays in different immune cells has started to reveal the coregulation of membrane lipids and innate immune responses (21–23). However, there are no functional lipidomic studies on primary DCs.

In this study, we used a shotgun lipidomics approach to elucidate the possible function of SWAP-70 in determining the lipid composition of CD11c$^+$ immune cells. We used LPS as a model of a pathogenic inflammatory stimulus (24, 25), and physical disruption of cell–cell contacts (CD) to represent a non-pathogenic stimulus leading to tolerance (6, 26, 27). Our data show characteristic changes in the lipidome of CD11c$^+$ immune cells upon their activation, and reveal an important role of SWAP-70 in the selective generation and localization of Cers.

Materials and Methods

Animals

Swap70$^{-/-}$ and isogenic *Swap70*$^{+/+}$ mice of two different strains 129/SvEMS and C57BL/6 were used (28, 29). Animals were bred and maintained under pathogen-free conditions in the Animal Facility of the Medical Faculty of the Dresden University of Technology according to approved animal welfare guidelines.

Bone marrow–derived DCs

Murine bone marrow–derived DCs (BMDCs) were obtained by differentiation of bone marrow–derived precursors as described previously (30) with small modifications. Femurs and tibiae were dissected from male *Swap70*$^{+/+}$ and *Swap70*$^{-/-}$ mice (6–10 mo of age) and bone marrow was flushed with supplemented RPMI 1640 using a 29-gauge syringe. Bone marrow cells were harvested by centrifugation and seeded at 0.25×10^6 cells per well of a six-well plate (non-tissue culture treated, *Sarstedt*) in 3 ml of supplemented RPMI 1640. Additionally, 10% of a GM-CSF containing cell culture supernatant was added to the culture. GM-CSF supernatant was routinely produced using the stably transfected cell line J558 (31) and generally led to a GM-CSF concentration of around 1 μg/ml as tested by ELISA (BD Biosciences) (data not shown). At day 3 of culture, an additional 3 ml of medium was added. Then half of the medium was changed every 2–3 d. BMDCs were analyzed at day 10 of culture unless otherwise stated, at which point >90% of the cells were CD11c positive as analyzed by FACS. BMDCs were defined as CD11c$^+$CD11b^{int} CD86^{high}. BMDCs were activated in a TLR-dependent manner by incubating the cells with 1 μg/ml LPS (*Salmonella enterica*; Sigma) for the indicated time points.

Supernatants of LPS-stimulated BMDCs were collected for analysis of cytokines IL-1α, IL-12p70, IL-6, and IL-10 using LEGENDplex (BioLegend) according to the manufacturer's instructions.

In some experiments, 0.1 μg/ml C3 Transferase (CT04 Rho Inhibitor I, *Cytoskeleton*) was added at day 3 of culture and kept until analysis. The drug was added freshly with each medium change under the assumption that remaining molecules were stable to keep the used concentration without big variations. Respective carriers were used as negative controls.

DCs were also generated in vitro by using the Flt3 ligand (Flt3-L) (eBioscience) as described (32). Briefly, total bone marrow cells (2×10^6/ml) were cultivated with 100 ng/ml of Flt3-L for 9 d. CD11c$^+$B220$^-$ CD11b$^-$ and CD11c$^+$B220$^-$CD11b$^+$ conventional DC populations were analyzed by FACS.

Shotgun lipidomics

Lipid extraction of cells was performed using a modified Folch protocol (33). Briefly, cells (the amount equivalent to 10 μg of total proteins) were diluted with 200 μl of 150 mM ammonium bicarbonate. Then 10 μl of an internal standard mixture containing 20 pmol triacylglycerol (TAG) 12:-12:0-12:0, 20 pmol diacylglycerol (DAG) 17:0-17:0, 40 pmol PC-*O*/-*O* 18:0-18-0, 50 pmol PE-*O*/-*O* 20:0-20:0, 10 pmol phosphatidylglycerol (PG) 17:0-17-0, 40 pmol phosphatidylserines 12:0-12:0, 50 pmol phosphatidylinositol (PI) 16:0-16:0, 40 pmol lysophosphatidylcholine 12:0, 40 pmol lysophosphatidylethanolamine 14:0, 40 pmol sphingomyelins (SM) 18:1;2-12:0;0, 20 pmol cholesteryl esters (CE) 12:0, 20 pmol Cer 18:1;2-12:0;0, and 50 pmol cholesterol d7 (all from Avanti Polar Lipids, Alabaster, AL) was added for the subsequent quantification. Then 265 μl of methanol and 730 μl of chloroform were added and the mixture was vortexed for 1 h at 4°C. The lower organic phase was collected and dried under vacuum. Lipid extract was redissolved in 120 μl chloroform/methanol mixture [1:2 (v/v)]. The lipidomics analysis was performed on a Q Exactive tandem mass spectrometer (Thermo Fisher Scientific, Bremen, Germany) equipped with a robotic nanoflow ion source TriVersa NanoMate (Advion BioSciences, Ithaca, NY) (34). Fourier transform mass spectrometry spectra were acquired for 1 min within the range of *m/z* 420–1000 in negative and *m/z* 450–1000 in positive mode at the target mass resolution of $R_{m/z\ 200}$ = 140,000 (full width at half maximum) and automated gain control settings of 10^6 ions. For the analyses in negative ion mode, 10 μl of lipid extract was mixed with either 12 μl of 13 mM ammonium acetate in isopropanol or 0.1% trimethylamine in methanol. For the analysis in positive mode, 10 μl extract was mixed with 90 μl 6.5 mM ammonium acetate in isopropanol before infusion. Lipids were identified and quantified using LipidXplorer software (35). Molecular Fragmentation Query Language queries were compiled for phosphatidylcholine, phosphatidylcholine ether (PC-O), lysophosphatidylcholine, phosphatidylethanolamine, phosphatidylethanolamine ether, lysophosphatidylethanolamine, PI, SM, TAG, DAG, Cer, cholesterol, CE, PG, phosphatidylserine, and phosphatidic acid lipid classes and are available at the LipidXplorer wiki site: https://wiki.mpi-cbg.de/lipidx/Main_Page. Cholesterol was quantified as previously described (36). Briefly, 30 μl of extract was dried under vacuum, then 75 μl acetyl chloride/chloroform [1:2 (v/v)] was added, incubated for 1 h at room temperature, dried under vacuum, and redissolved in 60 μl chloroform:methanol [1:2 (v/v)]. Then 10 μl extract was mixed with 90 μl 6.5 mM ammonium acetate in isopropanol before infusion, and analyzed in positive mode.

Cell separation by MACS

MACS cell separation (Miltenyi Biotec) was performed to isolate CD11c$^+$ cells used for shotgun lipidomics (see above). Cells from GM-CSF cultures were harvested after 10 d using ice-cold flow cytometry-buffer (2 mM EDTA + 0.1% BSA in PBS). Cells in this buffer were mixed with biotinylated Abs against CD11c and magnetically isolated using bead columns according to the manufacturer's recommendations. The isolated CD11c$^+$ cells were then resuspended at a concentration of 1×10^6 cells per ml in the same culture media for 24 h and referred to as cluster-disrupted cells (6). CD11c$^+$ cells from GM-CSF cultures stimulated with LPS (1 μg/ml) for 24 h were also isolated with MACS, used immediately for lipidomics analysis, and referred to as immunogenic cells.

Flow cytometry analysis

To analyze the surface expression of markers, floating and attached cells from GM-CSF cultures were harvested, washed once with ice-cold flow cytometry-buffer (see above), and stained with the following fluorescently labeled Abs (0.6–0.8 μg/ml) for 30 min on ice: anti-CD11c (clone N418), anti-CD86 (clone GL1), and anti-CD11b (clone M1/70) (all from eBioscience). Unlabeled anti-Cer (clone MID 15B4; Enzo) and anti-acid sphingomyelinase (H-181; Santa Cruz) were used as primary Abs. FITC- or APC-labeled secondary Abs were used (Jackson ImmunoResearch). Briefly, cells were fixed in 1% formaldehyde for 10 min, washed and incubated with anti-Cer or anti-acid sphingomyelinase Abs (1:30 dilution) at 37°C (Cers) or 4°C (acid sphingomyelinase) for 1 h, followed by incubation with secondary Abs (dilution 1:200) at 4°C for 30 min. Stained cells were washed once with flow cytometry buffer, resuspended, and analyzed on a BD LSRII (BD Biosciences) using FACSDiva software (BD Biosciences). Data were analyzed using FlowJo software (Tree Star).

Retroviral infection of BMDCs

GM-CSF cell cultures were transduced by retroviral infection. Retrovirus was produced by transiently transfecting the Phoenix Eco 293T retroviral packaging cell line using calcium phosphate/DNA precipitation combined with retroviral vectors (20 μg vector DNA per 10 cm dish of 80% confluent Phoenix cells). For the transduction, medium was changed to supplemented RPMI 1640 24 h posttransfection. The retrovirus containing supernatant was collected from Phoenix cell cultures at 48 h posttransfection and centrifuged once at $500 \times g$ for 5 min at 4°C to remove cell debris before infection of GM-CSF cell cultures. Transfected Phoenix cells were then used to produce the retrovirus for a second infection by adding fresh medium for another 24 h. Supernatant containing the retrovirus was always used fresh without freezing.

Downloaded from http://www.jimmunol.org/ by guest on February 24, 2022

Cells were transduced with retroviral vectors coding for c-terminally GFP-tagged SWAP-70. Cells were infected with supernatant containing retrovirus at days 3 and 4 of culture by passive incubation for 6–8 h at 37°C and 5% CO_2. The supernatant containing retrovirus produced was supplemented with 10% GM-CSF and 10 μg/ml polybrene before it was added to the cells. After 6–8 h of incubation, the supernatant containing retrovirus was removed from the cells and replaced with supplemented RPMI 1640 containing 10% GM-CSF. The infection procedure was repeated once. Cells were further cultured as described and analyzed at day 10.

Real time PCR

Total DC RNA was prepared by TRIzol lysis (Invitrogen). RNA was reversed transcribed into cDNA by using SuperScript II (Invitrogen). Expression of *Smpd1*, *Smpd2*, *Smpd4*, and *Ppp1R8* (control) was analyzed using a Rotor-Gene RG3000 (Qiagen) and the SYBR Green kit (Qiagen). The relative gene expression was calculated by dividing values to that of *Ppp1R8*. The primers were: *Smpd1* forward, 5′-ATCAACCTTAACCCTGGCTAC-3′; *Smpd1* reverse, 5′-TGGGTCAGATTCAAGATGTAGG-3′; *Smpd2* forward, 5′-TGCTTTCGTTGAGACTGAGG-3′; *Smpd2* reverse, 5′-TCAGAGACTGCCTTGTAAAGC-3′; *Smpd4* forward, 5′-AGACATCTGTGAATGCAGACC-3′; *Smpd4* reverse, 5′-AGACAGTGAGTCGGTAGTGTAG-3′; *Ppp1R8* forward, 5′-CGATCTGTGTGACTTCACTATCGA-3′; *Ppp1R8* reverse, 5′-AAAGTGCCATGTGTGCTGTTG-3′.

Acid-sphingomyelinase activity

Acid- and neutral sphingomyelinase activities were determined in DC lysates using a commercial fluorescent kit according to the manufacturer's instructions (Amplex Red Sphingomyelinase assay; Invitrogen).

Endosomal pH detection

Endosomal pH was detected using FITC- and Alexa 647-labeled 40 kDa dextran (Molecular Probes). BMDCs were pulsed with both dextrans at a concentration of 1 mg per ml for 15 min at 37°C and then washed with cold PBS. Cells were then chased for the indicated time points and immediately analyzed by flow cytometry. The ratio of the mean fluorescence intensity (MFI) of the two dyes was determined by flow cytometry. Binding of the dextrans at 4°C for 30 min in the presence of 1 μg/ml LPS was used as a negative control. Values were compared with a standard curve obtained by incubating the cells with the dextrans at a fixed pH in medium containing 0.01% Triton X-100. Cells were then immediately analyzed by flow cytometry to determine the ratio of MFI values at each pH.

Apoptosis assay

BMDCs were treated with 1 μg/ml LPS at the indicated time points in the presence or not of 20 μM C2 Cer (Calbiochem). Cells were then fixed and permeabilized in ice-cold ethanol and stained with 50 μg/ml propidium iodide. The apoptotic hypodiploid population in singlet cells was then determined by flow cytometry.

Confocal microscopy

For acid-sphingomyelinase and Lamp-1 staining, CD11c+ cells were left to adhere for 3 h on glass slides, then 1 μg/ml LPS was added to the cells and left for 30 min. Cells were fixed with 3.7% paraformaldehyde in PBS for 10 min at room temperature. Cells were then blocked with 3% BSA in PBS and permeabilized with 1% Triton X-100 (Sigma) in PBS. Acid-sphingomyelinase staining was done with unconjugated Abs (H-181; Santa Cruz) followed by Alexa Fluor 594-labeled Ab against rabbit IgG (Invitrogen).

Downloaded from http://www.jimmunol.org/ by guest on February 24, 2022

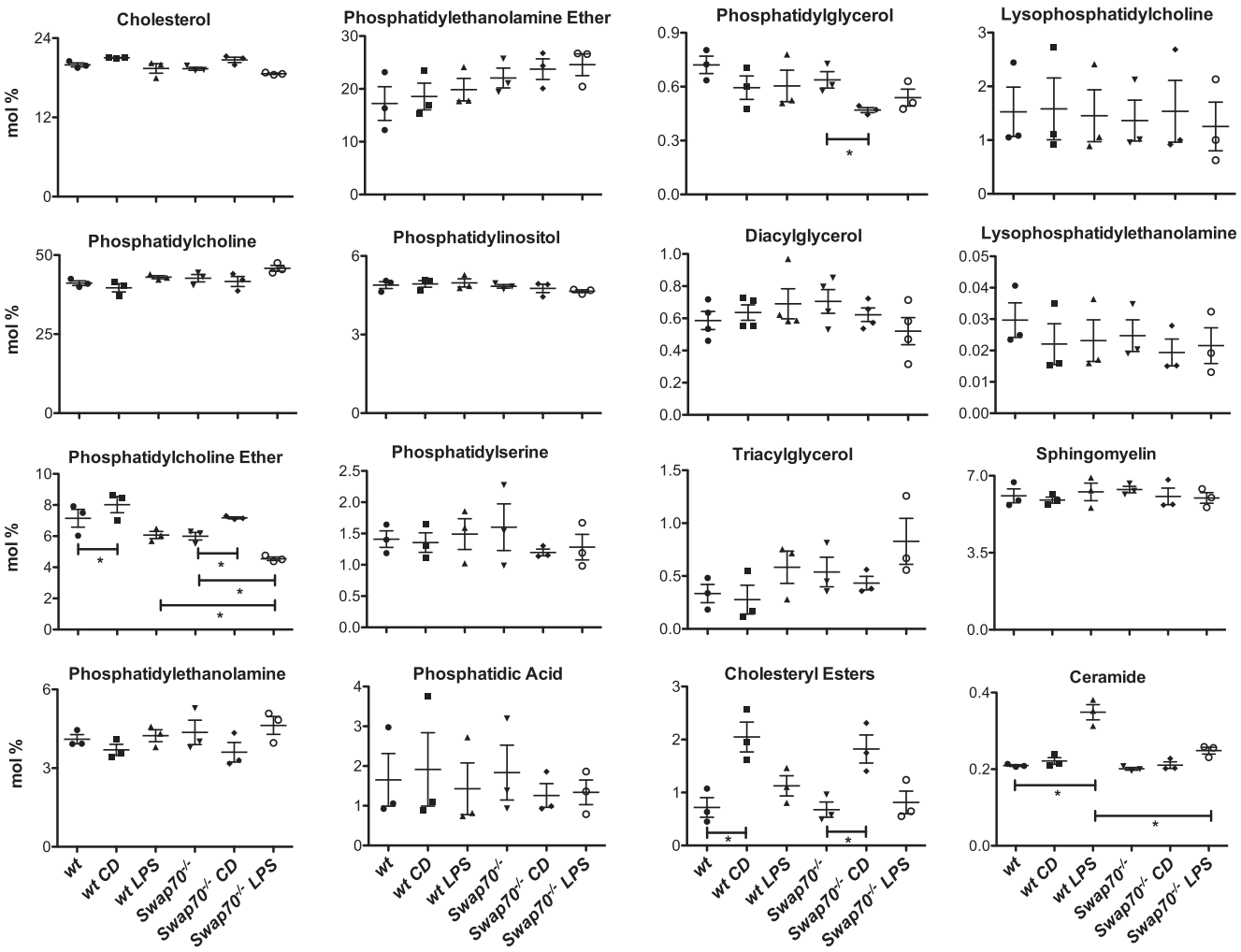

FIGURE 1. Lipidomic changes induced by two maturation mechanisms in CD11c+ immune cells from GM-CSF cultures. Lipid class compositions of CD11c+ cells that were stimulated with CD or bacterial LPS for 24 h. The content of each lipid class is the sum of the absolute abundance of all species in the lipid class from three independent experiments and is expressed as mol%. $*p < 0.05$.

Table I. Cer species (mean mol%) of non-stimulated (LPS−) and stimulated (LPS+) wt CD11c$^+$ cells

	LPS−	LPS+	*p* Value
Cer 32:1;2	0.003373774	0.004888668	0.0438
Cer 33:1;2	0.00639803	0.011796494	0.0264
Cer 34:1;2	0.077305125	0.142076397	0.0318
Cer 34:2;2	0.003357252	0.004197508	>0.05
Cer 35:1;2	0.001141359	0.003014037	0.0123
Cer 36:1;2	0.004354109	0.006883242	>0.05
Cer 38:1;2	0.003589288	0.005197015	>0.05
Cer 38:2;2	0.000326716	0.000384588	>0.05
Cer 39:1;2	0.000726604	0.001991341	>0.05
Cer 40:1;2	0.014583769	0.027501811	0.0275
Cer 40:2;2	0.003255224	0.005154889	0.0124
Cer 41:1;2	0.00532952	0.008384673	>0.05
Cer 41:2;2	0.007972497	0.012334424	0.0136
Cer 42:2;2	0.06916572	0.101486589	0.0117
Cer 42:3;2	0.008129199	0.012110741	0.0266
Cer 43:2;2	0.000484545	0.001319203	>0.05

Rat Alexa Fluor 488- labeled anti–Lamp-1 (1D4B; BioLegend) was used to visualize Lamp-1. Slides were mounted in Fluoromont-G (SouthernBiotech) and viewed using the Zeiss LSM 510 confocal microscopy system (Carl Zeiss). Imaging was performed using a 40×/1.3 DIC Oil objective. Lasers of 488 and 561 nm were used for excitation of FITC and Alexa Fluor-594 respectively. Emission wavelengths were separated by band passes 505–550 and >575 nm, respectively. Confocal sections of 1 μm per cell were taken. Colocalization of acid-sphingomyelinase and Lamp-1 was quantified according to previous studies (10, 16). Briefly, 40 cells were analyzed via ImageJ using the colocalization plug-in (ratio: 30%; threshold for each channel: 50). Nuclei were visualized with DAPI staining and an area around the surface of each cell in the colocalization image was analyzed for gray values representing the level of interaction of two proteins (values close to the maximum of 256 represent strong colocalization). Profiles for each cell showing the mean gray value per square micrometer were obtained, and the average of these mean values was plotted for acid-sphingomyelinase–Lamp-1 colocalization.

Lipid supplementation

Cers were purchased from Matreya and solubilized using ethanol/dodecane (21). Briefly, Cers dissolved in methanol were dried under vacuum and solubilized in ethanol/dodecane [ratio 98:2 (v/v)] by sonication for 30 min at 37°C and vortex every 5 min. For the supplementation studies, Cers (20 μM) were added to the cells 2 h before stimulation with LPS for 12 h.

Statistics

Statistical analysis and graphing were carried out with Prism 5 (GraphPad). ANOVA with Tukey post hoc test was employed to determine statistical significance.

Results

Specific lipidome dynamics induced by two distinct maturation mechanisms in CD11c$^+$ immune cells

In mammalian cells, phospholipids account for 60% of total lipids including phosphatidylcholine, phosphatidylethanolamines, PI, and phosphatidylserines. Other lipids classes like sphingolipids, such as SM and Cer, glycerolipids (TAG and DAG, respectively), and cholesterol range from 0.1 to 40% (37). We determined the lipid composition of murine GM-CSF–derived CD11c$^+$ immune cells by top-down shotgun lipidomics. Lipids were extracted by a modified Folch protocol (33) and analyzed on a Q Exactive tandem mass spectrometer (Thermo Fisher Scientific) (34). Lipid species were identified by their accurate masses and quantified using LipidXplorer software (35).

TLR activation using bacterial LPS was used as a pathogenic inflammatory stimulus, and physical disruption of cell–cell contacts, i.e., CD, represented a stimulus leading to tolerance. Similar to tolerogenic DCs induced by rapamycin and thymic stromal lymphopoietin (8, 9), CD-stimulated CD11c$^+$ cells produced fewer inflammatory cytokines, such as IL-1α, IL-12p70, and IL-6, but more anti-inflammatory IL-10 after LPS stimulus than cells that did not undergo CD (Supplemental Fig. 1A). This validated the tolerogenic capacity of physical disruption. The basal composition of the main lipid classes of CD11c$^+$ cells is similar to those of macrophages obtained in two lipidomics studies (38, 39) (Fig. 1). Fig. 1 also shows that the levels of 12 out of 16 lipid classes

Table II. Cer species (mean mol%) of non-stimulated (LPS−) and stimulated (LPS+) *Swap70*$^{-/-}$ CD11c$^+$ cells

	LPS−	LPS+	*p* Value
Cer 32:1;2	0.002742675	0.003224622	>0.05
Cer 33:1;2	0.005915743	0.007546661	>0.05
Cer 34:1;2	0.067189248	0.089022943	>0.05
Cer 34:2;2	0.00258713	0.002868257	>0.05
Cer 35:1;2	0.001056345	0.001874392	0.0042
Cer 36:1;2	0.004108222	0.005650391	0.0381
Cer 38:1;2	0.003333688	0.004141298	>0.05
Cer 38:2;2	0.000369403	0.000267582	>0.05
Cer 39:1;2	0.000608037	0.001643603	>0.05
Cer 40:1;2	0.012927915	0.020915018	>0.05
Cer 40:2;2	0.002897519	0.003552648	0.0233
Cer 41:1;2	0.00450518	0.006511649	0.0345
Cer 41:2;2	0.008569928	0.009905828	>0.05
Cer 42:2;2	0.075784784	0.082534552	>0.05
Cer 42:3;2	0.007632221	0.007729603	>0.05
Cer 43:2;2	0.000781396	0.001051803	>0.05

Downloaded from http://www.jimmunol.org/ by guest on February 24, 2022

Table III. Cer species (mean mol%) of LPS-stimulated wt and *Swap70*$^{-/-}$ CD11c^{+} cells

	Wt	*Swap70*$^{-/-}$	*p* Value
Cer 32:1;2	0.004888668	0.003224622	>0.05
Cer 33:1;2	0.011796494	0.007546661	0.0043
Cer 34:1;2	0.142076397	0.089022943	0.0233
Cer 34:2;2	0.004197508	0.002868257	>0.05
Cer 35:1;2	0.003014037	0.001874392	0.0225
Cer 36:1;2	0.006883242	0.005650391	>0.05
Cer 38:1;2	0.005197015	0.004141298	>0.05
Cer 38:2;2	0.000384588	0.000267582	>0.05
Cer 39:1;2	0.001991341	0.001643603	>0.05
Cer 40:1;2	0.027501811	0.020915018	0.0366
Cer 40:2;2	0.005154889	0.003552648	0.0042
Cer 41:1;2	0.008384673	0.006511649	>0.05
Cer 41:2;2	0.012334424	0.009905828	0.0184
Cer 42:2;2	0.101486589	0.082534552	0.0160
Cer 42:3;2	0.012110741	0.007729603	0.0062
Cer 43:2;2	0.001319203	0.001051803	>0.05

remained unchanged in non-stimulated CD11c^{+} cells and in cells stimulated with either LPS or CD. These lipids, which include SM, were not different between wt and *Swap70*$^{-/-}$ CD11c^{+} cells, left unstimulated or stimulated in the same manner (Fig. 1).

After 24 h of CD or LPS treatment, we observed statistically significant differences in four classes of lipids between the two activation stimuli and between wt and *Swap70*$^{-/-}$ CD11c^{+} cells (Fig. 1). CD but not LPS led to an increase of PC-O and CE in both wt and *Swap70*$^{-/-}$ CD11c^{+} cells. This affected the abundance of approximately half of the individually quantified PC-O and CE species (Supplemental Table IA, IB). PC-O species with 30–35 atoms of carbon in their fatty acid and fatty alcohol moieties were downregulated, whereas species with more than 35 carbon atoms were upregulated (Supplemental Table IA, IB). In addition, there was a significant difference in the mol% of PC-O after LPS stimulus between wt and *Swap70*$^{-/-}$ cells (Fig. 1). The mol% of CE increased after the CD stimulus to similar levels, more than 2-fold, in wt and *Swap70*$^{-/-}$ CD11c^{+} cells (Fig. 1, Supplemental Table IC, ID). Only in *Swap70*$^{-/-}$ cells we also observed a statistically significant reduction of the levels of PG upon CD but not LPS treatment (Fig. 1).

In stark contrast to wt cells, *Swap70*$^{-/-}$ CD11c^{+} cells failed to significantly increase their Cer content after LPS activation. Wt cells showed a clear increase of almost 2-fold in their Cer content after LPS stimulation, but *Swap70*$^{-/-}$ CD11c^{+} cells did not. Wt and *Swap70*$^{-/-}$ cells did not show a significant difference in their total Cer content before the addition of LPS (Fig. 1). Table I shows that after LPS addition, wt cells increase the concentration of all Cer species, with nine (56.3%) showing statistically significant differences. The numbers of carbon atoms of these Cers are in the range of 32–35 and 40–42. With exception of Cer 38:2;2, there was also an increase in the Cer species in *Swap70*$^{-/-}$ cells after LPS activation (Table II). However, only four (25%) showed statistically significant differences: Cer 35:1;2, Cer 36:1;2, Cer 40:2;2, and Cer 41:1;2 (Table II). The two species contributing most to the overall Cer content, Cer 34:1;2 and Cer 42:2;2, were

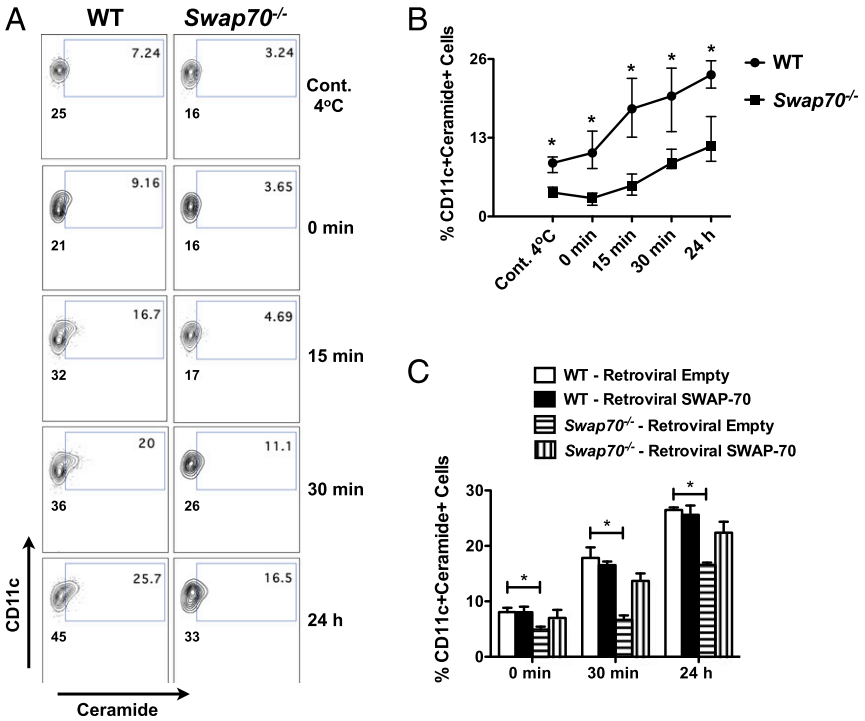

FIGURE 2. SWAP-70 controls Cer accumulation at the surface of CD11c^{+} immune cells. (**A**) Flow cytometry dot plots of CD11c^{+} cells at different time points after addition of 10 μg/ml LPS. Numbers in the gates represent the percentage of CD11c^{+}Cer^{+} cells. Numbers outside the gates represent the MFI of Cer staining. CD11c^{+} cells incubated with LPS for 30 min on ice were used as negative control (Cont. 4°C). Only one representative experiment is shown. (**B**) Averages of the CD11c^{+}Cer^{+} cell percentage of at least five independent experiments. (**C**) Three-day CD11c^{+} cells were transfected with SWAP-70-GFP by retroviral infection and GFP^{+} cells were analyzed at day 10 to determine the percentage of CD11c^{+}Cer^{+} cells. Retroviral infection with GFP alone (empty vector) was used as negative control. *$p < 0.05$.

Downloaded from http://www.jimmunol.org/ by guest on February 24, 2022

increased in wt and *Swap70*$^{-/-}$ CD11c^{+} cells after LPS but only in wt the difference in both Cers was statistically significant (Tables I, II). Table III shows that 50% of Cer species (including Cer 34:1;2 and Cer 42:2;2) in *Swap70*$^{-/-}$ cells were significantly reduced after the LPS stimulus when compared with wt. Taken together, these results indicate that SWAP-70 plays an important role in controlling the increase of Cers in CD11c^{+} cells after stimulation by LPS. CD, however, did not change Cer levels in these cells, whether SWAP-70 proficient or deficient. This illustrates the activation pathway–specific nature of Cer dynamics.

As mentioned above, 2 out of 16 Cer species, Cer 34:1;2 and Cer 42:2;2, contributed around 40 and 30%, respectively, to the total Cer content of CD11c^{+} cells (Tables I, II). To test the impact of these two Cers in the LPS-induced cytokine production of these cells, we used lipid supplementation studies. Supplemental Fig. 2 shows that addition of Cer 34:1;2 before activation with LPS led to an inhibition in the production of cytokines IL-1α, IL-12p70, IL-10, and IL-6. With an exception of a decrease in the production of IL-10 (albeit not significant), Cer 42:2;2 has no effect in the production of IL-1α, IL-12p70, and IL-6 (Supplemental Fig. 1B). This observation suggests different effects of Cer species in cytokine production after signaling through an LPS stimulus.

To our knowledge, these results indicate for the first time that two different pathways of activation, immunogenic and tolerogenic, induce different changes in the levels of specific lipid classes of cultured CD11c^{+} cells. It will therefore be of great interest to clarify the contributions of PC-O, CE, PG, and Cer in immunogenic versus tolerance reactions.

SWAP-70 controls LPS-induced Cer accumulation at the surface of DCs

The generation of Cer at the plasma membrane can be induced upon certain stimuli as a result of activation of acid sphingomyelinase residing in endosomes and lysosomes that are directed and fused to the plasma membrane (40–43). In DCs, accumulation of Cers in the plasma membrane occurs a few minutes after C-type lectin receptor and TLR stimuli (40, 44). With flow cytometry (FACS) we analyzed whether addition of LPS leads to an increase of Cer-positive cells in fixed, non-permeabilized DCs reflecting the accumulation of Cers in their plasma membrane. Wt and *Swap70*$^{-/-}$ CD11c^{+} cells were analyzed at different time points after LPS activation. Fig. 2A and 2B shows the increase of wt Cer-positive CD11c^{+} cells 15 and 30 min after the stimulus with LPS, and they remained high after 24 h. There is also an increase in the frequency of *Swap70*$^{-/-}$ Cer-positive cells at every time point but at much reduced values, often less than half, when compared with wt cells (Fig. 2A, 2B). The frequency of wt Cer-positive cells was ~2-fold higher than that of *Swap70*$^{-/-}$ CD11c^{+} cells (Fig. 2B). The increase in the MFI of the Cer staining during LPS treatment indicates that all cells responded to stimulation and this intensity was always lower in *Swap70*$^{-/-}$ CD11c^{+} cells (Fig. 2A, numbers outside gates).

Although the basal, preactivation surface Cer accumulation in *Swap70*$^{-/-}$ CD11c^{+} cells is already significantly reduced, the total cell Cer concentration reflects wt levels (Fig. 1). This indicates that non-stimulated *Swap70*$^{-/-}$ CD11c^{+} cells have a problem in localizing Cer on their surface rather than in producing normal levels of Cer. The FACS data (Fig. 2) further revealed that there is an exacerbated reduction of Cer on the surface of SWAP-70–deficient

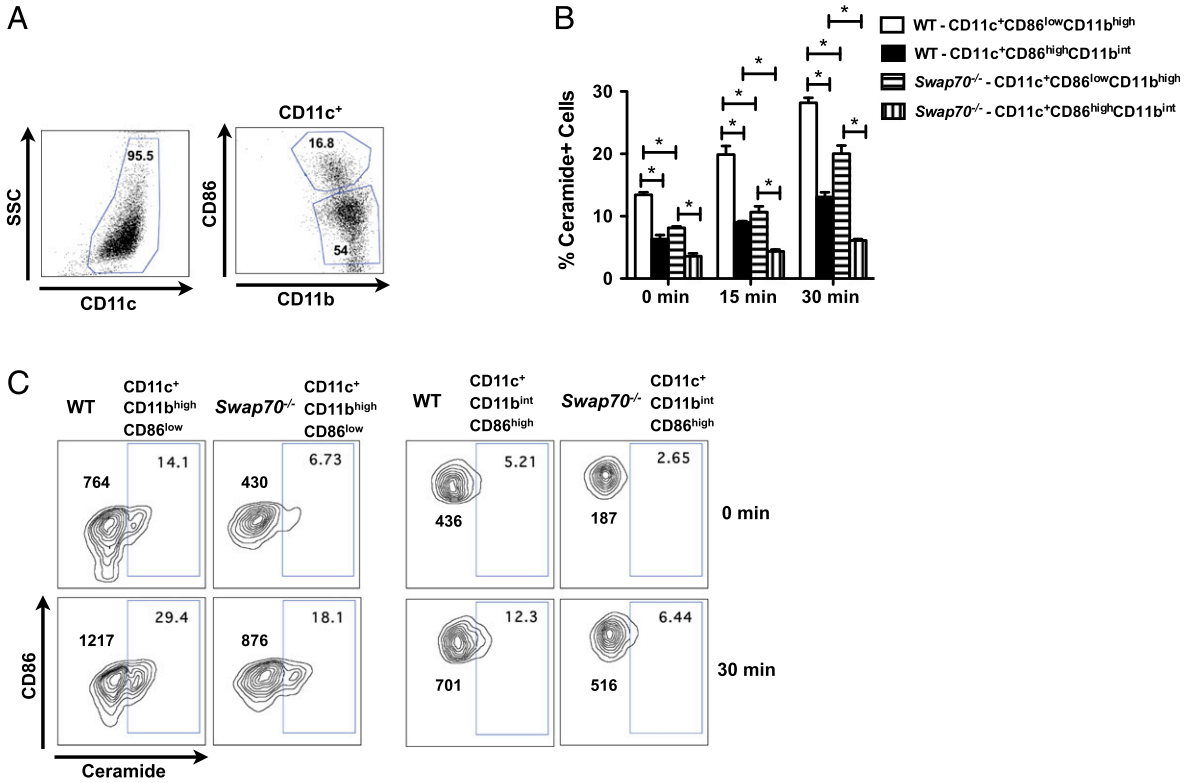

FIGURE 3. *Swap-70*$^{-/-}$ GM-CSF–generated DCs express less surface Cer. (**A**) Dot plots used to distinguish the mixed (CD11c^{+}CD86^{low}CD11b^{high}) and DC (CD11c^{+}CD86^{high}CD11b^{int}) populations in GM-CSF cultures at day 10. Numbers in the gates represent the percentage of CD11c^{+} cells (left panel) and the percentages of mixed (CD11c^{+}CD86^{low}CD11b^{high}) and DC (CD11c^{+}CD86^{high}CD11b^{int}) populations (right panel). Only one representative experiment is shown. (**B**) Dot plots of mixed and DC populations at 0 min and 30 min after addition of 10 μg/ml LPS. Numbers in the gates represent the percentage of Cer^{+} cells for each population. Numbers outside the gates represent the MFI of Cer staining. Only one representative experiment is shown. (**C**) Averages of the percentage of mixed and DC populations positive for Cer cells of at least three independent experiments. $^{*}p < 0.05$.

Downloaded from http://www.jimmunol.org/ by guest on February 24, 2022

CD11c$^+$ cells at every time point after LPS stimulation, in line with the reduced concentration Cers observed in *Swap70*$^{-/-}$ cells after exposure to LPS for 24 h (Fig. 1). Thus, after stimulation there is not only a deficiency in the ability to accumulate Cer on the cell surface, but to produce or maintain normal levels of Cer. To confirm the SWAP-70 dependency of surface Cer accumulation, we expressed full-length SWAP-70 in CD11c$^+$ cells through a retroviral infection system used in our previous studies (10, 15, 16). Fig. 2C shows that expression of SWAP-70 in *Swap70*$^{-/-}$ cells restored the accumulation of Cer in the plasma membrane to nearly wt levels. Overexpression of SWAP-70 in wt cells did not affect the number of surface Cer-positive cells.

Recent studies have shown that CD11c$^+$ cells in GM-CSF cell cultures consist of two populations: a first of mature DCs (CD11c$^+$CD86^{high}CD11b^{int}) and a second (CD11c$^+$CD86^{low}CD11b^{high}) of immature DCs, macrophage-like, and progenitor cells [(4, 45–47), Fig. 3A]. We sorted both populations followed by LPS activation to determine the Cer on their plasma membrane. These attempts, however, failed to induce Cer accumulation, probably due to an inhibitory effect arising from the disruption of cell–cell contacts (CD) needed to prepare the cells for sorting before LPS stimulus (data not shown). Instead, we have analyzed the Cer accumulation in the membrane of the two populations (Fig. 3A) at the early 15 min and 30 min time points after LPS addition. Fig. 3B and 3C show that the mixture of immature DCs, macrophage-like, and progenitor cells in these cultures generally generated more Cer on their surface than mature DCs. Importantly, both *Swap70*$^{-/-}$ populations display significantly reduced numbers of surface Cer-positive cells (and Cer MFI) before and after LPS stimulus when compared with wt. The differences were about the same for both cell types. To further test the SWAP-70 deficiency in the accumulation of surface Cer on DCs, we used Flt3-L in vitro cultures to generate conventional DCs from bone marrow precursors followed by activation with LPS for 30 min (32). In these cultures, the subset CD11c$^+$B220$^-$CD11b$^-$ cells is homologous to CD8α$^+$ DCs, and CD11c$^+$B220$^-$CD11b$^+$ is to CD8α$^-$ DCs (Fig. 4A) (32). As observed in the GM-CSF cultures, both *Swap70*$^{-/-}$ DCs populations showed a significant decrease in the accumulation of Cer at all time points when compared with their wt counterparts (Fig. 4B, 4C). Taken together, these results further highlight the importance of SWAP-70 in the mechanism of Cer accumulation on the cell surface of DCs after LPS activation.

Swap70$^{-/-}$ *CD11c*$^+$ *immune cells fail to activate and translocate acid sphingomyelinase to the plasma membrane after LPS activation*

After contact with viruses or LPS, DCs generate surface Cer through the hydrolysis of sphingomyelin, which is present in the cells at levels at least a magnitude higher than Cer [(48), Fig. 1], by sphingomyelinases (40, 44). De novo synthesis of Cer is a slower process, playing a minor role in the acute generation of Cers upon signaling by stimuli like LPS (40, 48–50). Whole-genome transcriptome analysis of wt and *Swap70*$^{-/-}$ DCs identified the following sphingomyelinases expressed in these cells: acid sphingomyelinase (*Smpd1*), neutral sphingomyelinase (*Smpd2*), and neutral sphingomyelinase 3 (*Smpd4*) (data not shown). We analyzed the basal expression levels of these enzymes by PCR in wt and *Swap70*$^{-/-}$ CD11c$^+$ immune cells and at different time

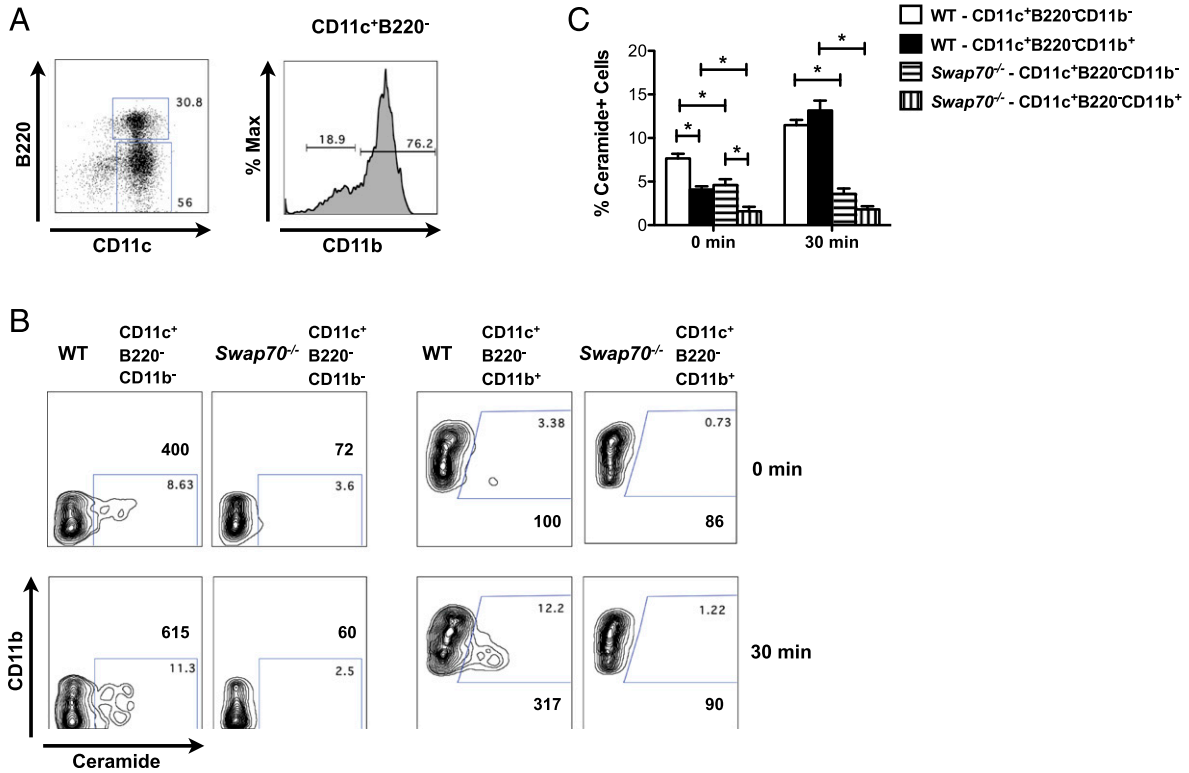

FIGURE 4. *Swap-70*$^{-/-}$ Flt3-L–generated DCs express less surface Cer. (**A**) FACS staining used to distinguish (CD11c$^+$B220$^-$CD11b$^-$) and (CD11c$^+$B220$^-$CD11b$^+$) DC populations in Flt3-L cultures at day 9. Numbers in the gates represent the percentage of CD11c$^+$B220$^+$ and CD11c$^+$B220$^-$ cells (left dot plot) and percentages of (CD11c$^+$B220$^-$CD11b$^-$) and (CD11c$^+$B220$^-$CD11b$^+$) DC populations (right histogram). Only one representative experiment is shown. (**B**) Dot plots of (CD11c$^+$B220$^-$CD11b$^-$) and (CD11c$^+$B220$^-$CD11b$^+$) DC populations at 0 and 30 min after addition of 10 μg/ml LPS. Numbers in the gates represent the percentage of Cer$^+$ cells for each population. Numbers outside the gates represent the MFI of Cer staining. Only one representative experiment is shown. (**C**) Averages of the percentage of (CD11c$^+$B220$^-$CD11b$^-$) and (CD11c$^+$B220$^-$CD11b$^+$) DC populations positive for Cer cells of at least three independent experiments. $*p < 0.05$.

Downloaded from http://www.jimmunol.org/ by guest on February 24, 2022

points after exposure to LPS. Supplemental Fig. 3 shows no difference in the expression of the sphingomyelinases between wt and *Swap70*$^{-/-}$ cells. These results suggest that the reduced Cer accumulation observed in *Swap70*$^{-/-}$ cells is not due to variations in the expression of sphingomyelinases. The data also show that LPS activation of CD11c^{+} cells induces rapid downregulation of *Smpd1*, *Smpd2*, and *Smpd4* expression (Supplemental Fig. 2) as also reported in studies using RAW macrophages (21). This indicates that activity of sphingomyelinases and not their expression is the key mechanism leading to Cer accumulation after LPS stimulus (44). The above results suggest a failure to activate sphingomyelinases by *Swap70*$^{-/-}$ cells. We analyzed the activity of sphingomyelinase 30 and 60 min after LPS addition to the cells. We used an assay that continuously measures sphingomyelinase activity under a near-neutral or acidic pH environment, corresponding to the activities of the two neutral sphingomyelinases (*Smpd2* and *Smpd4*), and acid sphingomyelinase (*Smpd1*), respectively. Fig. 5A shows increased acid-sphingomyelinase activity at 30 min only in wt and not in *Swap70*$^{-/-}$ CD11c^{+} cells, returning to basal level activity at 60 min. The same stimulus led to a moderate decrease in neutral-sphingomyelinases activity at 30 min only in wt cells with no change in *Swap70*$^{-/-}$ cells (Fig. 5A). The results agree with a previous publication reporting increased activation of acid and not of neutral sphingomyelinases in DCs after an LPS stimulus (44). Degradation of SM by acid-sphingomyelinase takes place in the acidic environment of late endosomes and lysosomes and its optimal pH ranges between 4.5 and 5.5, but it can also hydrolyze raft-associated SM in the plasma membrane at around neutral pH (49). To measure the endosomal pH in wt and in *Swap70*$^{-/-}$ cells, we used 40 kDa dextran labeled with FITC (pH sensitive) or with AlexaFluor 647 (pH insensitive) (51). Briefly, cells were pulsed with both labeled dextrans, washed, followed by a chase for the indicated periods of time, and immediately analyzed by FACS. We determined then the ratio of the MFI of the two dyes. Values were compared with a standard curve obtained by wt cells that had endocytosed dextran at a fixed pH (Supplemental Fig. 3A). As shown in Fig. 5B, LPS led to a decrease of endosomal pH in wt cells throughout the treatment with the lowest value reached at 30 min. *Swap70*$^{-/-}$ cells, on the contrary, were not able to decrease their endosomal pH after addition of LPS (Fig. 5B) and thus would not provide the optimal acidic environment for the activity of acid sphingomyelinase. These results suggest that failure to activate acid sphingomyelinase in *Swap70*$^{-/-}$ CD11c^{+} cells leads to the reduced accumulation of Cer after LPS stimulus.

Acid sphingomyelinase is cotransported from lysosomal compartments upon C-type lectin receptor stimulus to the plasma membrane in DCs and there it can hydrolyze raft-associated SM (40). To investigate if CD11c^{+} cells in our cultures also transfer acid sphingomyelinase to the plasma membrane after LPS treatment, we analyzed the presence of acid sphingomyelinase in the cell membrane of fixed and non-permeabilized cells by FACS before and 30 min after the stimulus with the TLR ligand. Fig. 6A and 6B show a more than 2-fold increase of acid sphingomyelinase–positive wt cells after LPS stimulus. *Swap70*$^{-/-}$ CD11c^{+} cells show only a 1.6-fold increase after LPS stimulus and, before LPS treatment, about half of acid-sphingomyelinase positive cells compared with wt cells (Fig. 6A, 6B). The MFI of the sphingomyelinase staining also shows reduced expression (Fig. 6A, red numbers). Colocalization analysis by confocal microscopy of acid sphingomyelinase with the lysosomal marker Lamp-1 in wt CD11c^{+} cells upon stimulation with LPS shows strong colocalization of the two proteins on the surface (Fig. 6C) as shown by the levels of gray values representative of interaction (Fig. 6C, 6D). In agreement with the FACS analysis, there was a modest but significant increase in the level of surface interaction between acid sphingomyelinase and Lamp-1 in *Swap70*$^{-/-}$ CD11c^{+} cells after the LPS stimulus (Fig. 6C, 6D). Taken together, these results suggest that SWAP-70 controls Cer accumulation at the cell membrane

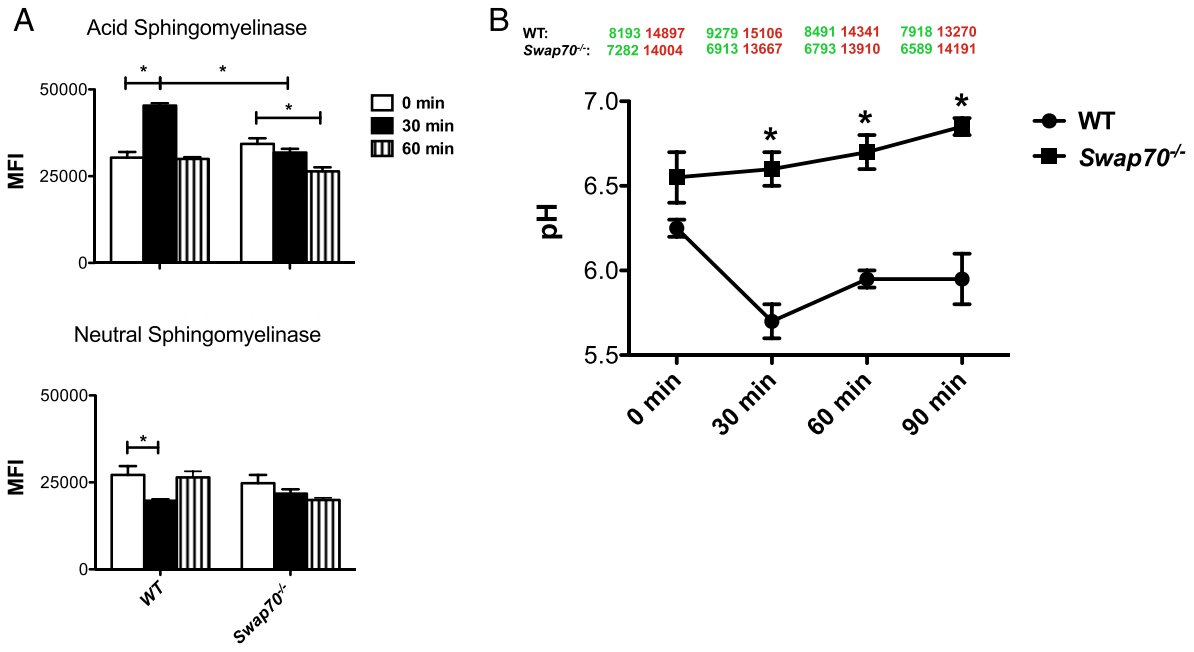

FIGURE 5. *Swap70*$^{-/-}$ CD11c^{+} immune cells fail to activate acid sphingomyelinase and to lower the endosomal pH after LPS activation. (**A**) Whole-cell lysates of CD11c^{+} cells exposed to LPS at the indicated time points were used to determine acid and neutral sphingomyelinase activity using a commercial kit. Averages of MFI of at least three independent experiments are shown. (**B**) Endosomal pH kinetics of CD11c^{+} after a 15-min pulse with dyes and the indicated time points of chase. Averages of at least three independent experiments are shown. The values on top represent the average of the mean fluorescence intensity of FITC (green) and AlexaFluor 647 (red) as measured by flow cytometry. *$p < 0.05$.

Downloaded from http://www.jimmunol.org/ by guest on February 24, 2022

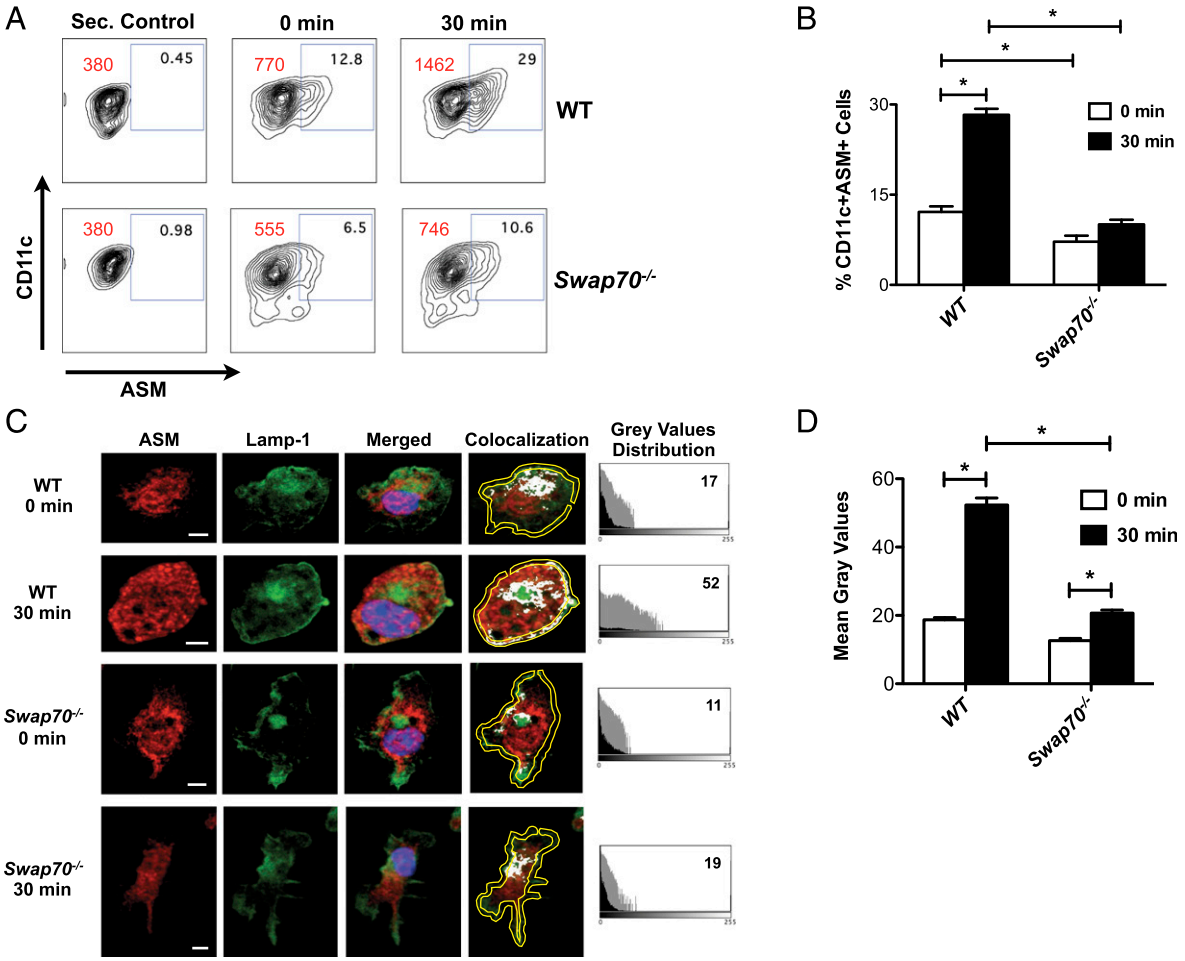

FIGURE 6. *Swap70*$^{-/-}$ CD11c^{+} immune cells fail to translocate acid sphingomyelinase (ASM) at the plasma membrane. (**A**) Dot plots of DCs at different time points after addition of 10 μg/ml LPS. Numbers in the gates represent the percentage of CD11c^{+}ASM^{+} cells. Red numbers outside the gates represent the MFI of acid sphingomyelinase staining. CD11c^{+} cells incubated only with secondary control Ab were used as negative control. Only one representative experiment is shown. (**B**) Averages of the CD11c^{+}ASM^{+} cell percentage of at least five independent experiments. (**C**) Colocalization images show gray spots representing interaction of the two proteins. An area around the surface (yellow line) was drawn for quantification of gray values. Scale bar, 2 μm. Histograms show the distribution of gray values per square micrometers for the colocalization images. (**D**) The average of the mean gray values per square micrometer obtained from all of the histograms (40 for each staining) analyzed. Data are representative of at least two independent experiments. $*p < 0.05$.

through two mechanisms: first, control of acid-sphingomyelinase activity after LPS stimulus through endo-lysosome maturation by lowering endosomal pH. Second, control of a transport mechanism of endosomal contents to the plasma membrane independent of TLR signaling leading to the proper localization of acid sphingomyelinase and the accumulation of Cers in the cell membrane compartment.

Inhibition of activated RhoA in Swap70$^{-/-}$ *CD11c*$^{+}$ *immune cells restored accumulation of surface Cer and cell membrane translocation of acid sphingomyelinase*

Our previous studies have demonstrated that SWAP-70 and RhoGTPases functionally interact in the control of the transport of endosomal MHCII-containing compartments to the cell membrane (10). Constitutive RhoA activation in *Swap70*$^{-/-}$ DCs was responsible for the failure to transport the MHCII vesicles and the inhibition of this premature RhoA activation restored their capacity to translocate MHCII-containing endosomes to the surface membrane (10). We therefore investigated whether constitutively active RhoA plays a role in the failure to bring acid sphingomyelinase to the plasma membrane, resulting in lower accumulation of Cer on *Swap70*$^{-/-}$ cells (see Figs. 2A, 2B, 6). We added the exoenzyme C3 ADP-ribosyltransferase (C3) at a low concentration (0.1 μg/ml) at day 3 of culture and maintained it until LPS activation at day 10. Using biochemical and imaging assays, we earlier demonstrated that this treatment leads to RhoA inactivation in *Swap70*$^{-/-}$ CD11c^{+} cells with no effect on wt cells (10, 16). Fig. 7A and 7B show that inactivation of RhoA in *Swap70*$^{-/-}$ cells restored their surface Cer to wt levels at all time points and that C3-treated *Swap70*$^{-/-}$ cells exposed significantly more Cer on their surface than untreated *Swap70*$^{-/-}$ cells. In addition, C3 treatment led to a significantly higher level of Cer in *Swap70*$^{-/-}$ CD11c^{+} cells at 24 h when compared with their wt counterparts. Further, the exoenzyme treatment had no effect on wt cells. We next investigated if inhibition of RhoA activation can also improve the translocation of acid sphingomyelinase to the cell membrane after the LPS stimulus in *Swap70*$^{-/-}$ cells. Indeed, C3 treatment significantly improves the surface localization of acid sphingomyelinase before and after addition of LPS (Fig. 7C). These results indicate that the control of RhoA activation by SWAP-70 is central to the surface accumulation of Cer in CD11c^{+} cells before and after LPS stimulus by regulating the necessary transport of acid sphingomyelinase to the cell membrane.

Downloaded from http://www.jimmunol.org/ by guest on February 24, 2022

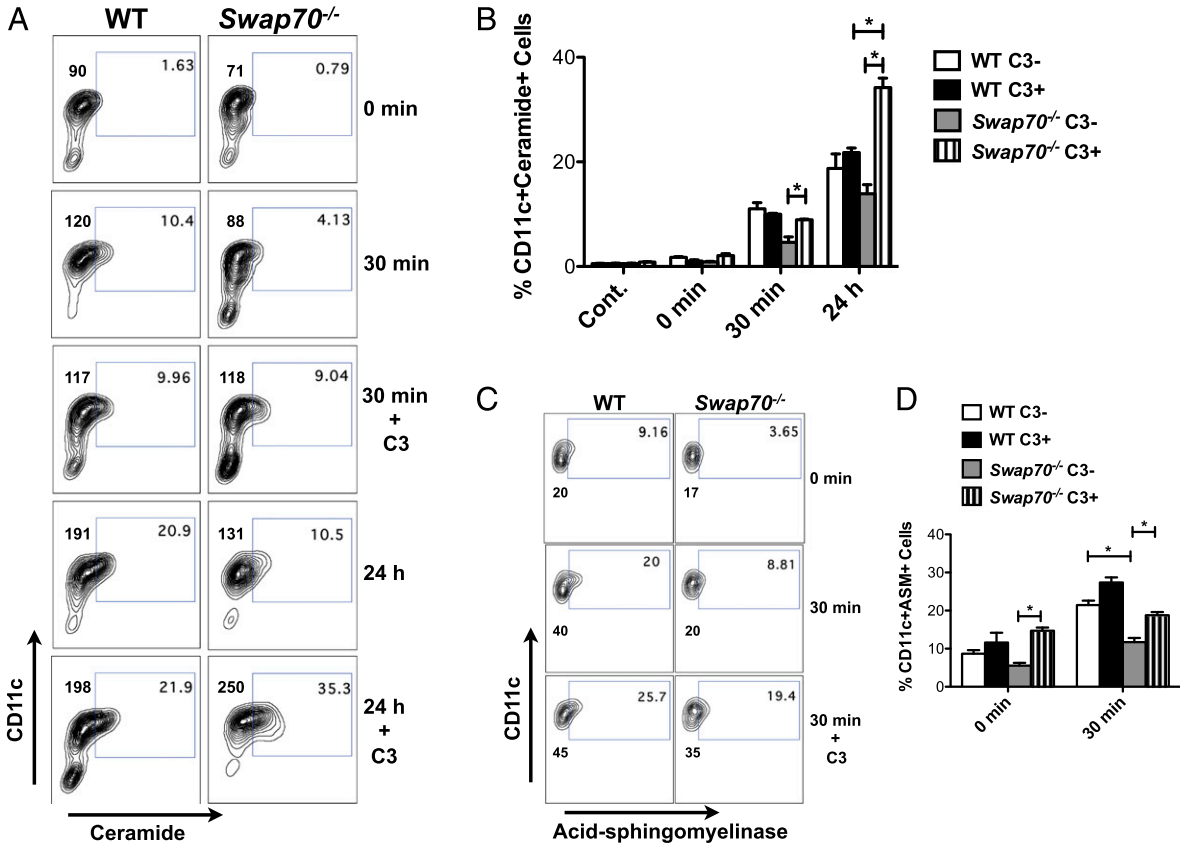

FIGURE 7. Inhibition of activated RhoA in *Swap70*$^{-/-}$ CD11c^{+} immune cells increases the accumulation of surface Cer to wt levels and translocation of acid sphingomyelinase in cell membrane. (**A**) Dot plots of DCs at different time points after addition of 10 μg/ml LPS incubated or not with C3 ADP-ribosyltransferase (C3). Numbers in the gates represent the percentage of CD11c^{+}C^{+} cells. Numbers outside the gates represent the MFI of Cer staining. Only one representative experiment is shown. (**B**) Averages of CD11c^{+}Cer^{+} cells percentage of at least three independent experiments. (**C**) Dot plots of DCs at different time points after addition of 10 μg/ml LPS incubated or not with C3 ADP-ribosyltransferase (C3). Numbers in the gates represent the percentage of CD11c^{+}ASM^{+} cells. Numbers outside the gates represent the MFI of acid sphingomyelinase staining. Only one representative experiment is shown. (**D**) Averages of CD11c^{+}ASM^{+} cells percentage of at least three independent experiments. $^{*}p < 0.05$.

Reduced apoptosis of Swap70$^{-/-}$ *CD11c*$^{+}$ *immune cells after LPS stimulus*

Previous reports have shown that Cers enhance the apoptotic effect of LPS in endothelial cells and DCs (44, 52) and exogenous Cer has proapoptotic effects in different cell types (53). To establish a functional phenotype related to the failure to accumulate Cer, we used FACS to investigate the frequency of apoptotic wt and *Swap70*$^{-/-}$ CD11c^{+} cells after LPS stimulus by the appearance of a hypodiploid DNA peak in PI-stained cells. We also analyzed the effect of exogenously added Cer on apoptosis of the cells. Fig. 8A and 8B show the number of apoptotic cells 48 h after LPS addition where *Swap70*$^{-/-}$ cells had a significant reduction in apoptosis when compared with LPS-treated wt. Importantly, this difference was abrogated with the addition of exogenous Cer (C2). The rates of apoptosis 24 h after LPS activation did not reveal differences between wt and *Swap70*$^{-/-}$ CD11c^{+} cells (data not shown). Fig. 8B also shows the apoptotic effect of Cer alone, with a significant increase in *Swap70*$^{-/-}$ cells before LPS addition, as shown in other cell types (53). To test if expression of SWAP-70 in *Swap70*$^{-/-}$ cells leads to an increase of apoptosis, *Swap70*$^{-/-}$ CD11c^{+} cells expressing SWAP-70 from a retroviral expression vector (see Fig. 2C) were stimulated with LPS and their apoptosis was analyzed after 48 h. The expression of SWAP-70 significantly increased the percentage of apoptotic cells in *Swap70*$^{-/-}$ cells. Overexpression of SWAP-70 in wt cells did not increase apoptosis (Supplemental Fig. 3B). Taken together, these results indicate a functional link between poor Cer accumulation and reduced apoptosis in *Swap70*$^{-/-}$ CD11c^{+} cells.

Discussion

Lipids play important roles in a wide range of biological processes of cells and organisms and the study of cellular lipid composition is central to deciphering the mechanisms involved in such processes (20, 37). However, studies of the lipid changes occurring during DC maturation are scarce (54), and there is no systematic lipidomics. In this report, we show that lipid dynamics are specifically different for cells undergoing maturation leading either to tolerance or inflammation.

We used physical CD of cell–cell interactions in CD11c^{+} cells of GM-CSF cultures as described by others (6, 26, 27) as a model for the tolerance-type of maturation. This stimulus led to upregulation of PC-O and CE, which were not observed as upregulated during inflammatory maturation triggered by LPS. In human leukocytes, PC-O are ether lipids mostly in alkylacylglycerophosphocholine form (55). In human macrophages, alkylacylglycerophosphocholines can serve as precursors in the remodelling pathway for the synthesis of platelet-activating factor (PAF), a lipid mediator involved in all proinflammatory reactions (56). Rapid production of PAFs through the remodelling pathway was also observed in LPS-stimulated murine macrophages (57, 58). Accumulation of PC-O may thus indicate an absence of PAF production after the protolerant CD stimulus. We observed decreased levels of PC-O after LPS stimulus, albeit only significantly different in *Swap70*$^{-/-}$

Downloaded from http://www.jimmunol.org/ by guest on February 24, 2022

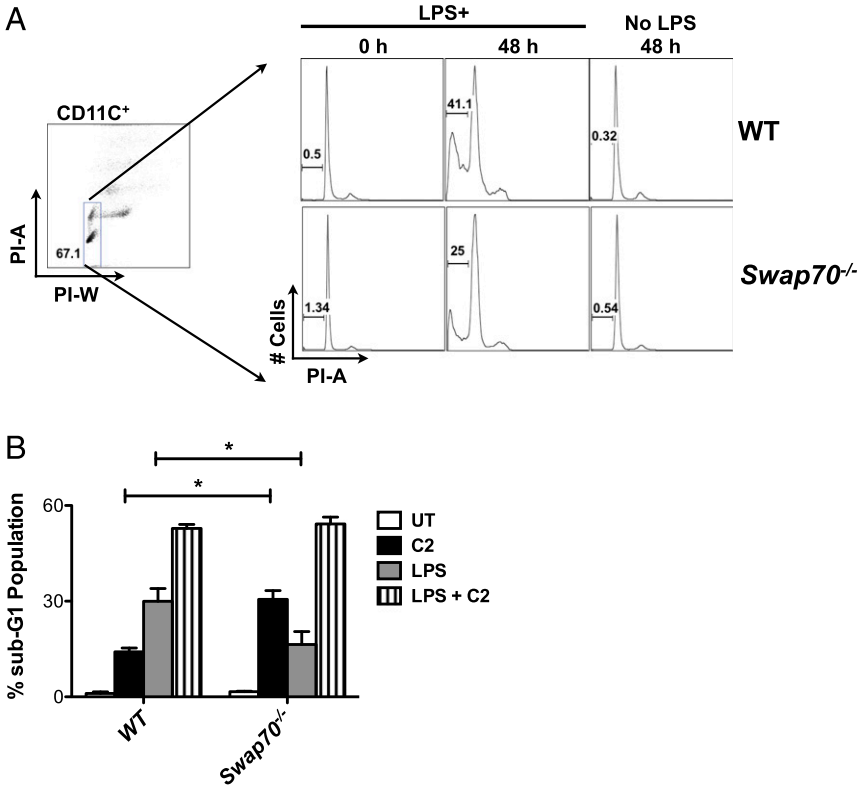

FIGURE 8. *Swap70*$^{-/-}$ CD11c$^+$ immune cells show reduced apoptosis after LPS stimulus. (**A**) DNA content analyzed by flow cytometry measuring the binding of propidium iodide (PI) in permeabilized cells. Left panel shows the dot plot used to distinguish singlet cells (percentage shown next to the gate). Right panels show the percentages of sub-G_1 hypodiploid apoptotic singlet CD11c$^+$ cells incubated with 10 μg/ml LPS at different time points. (**B**) Averages of the percentages of sub-G_1 cells incubated with 10 μg/ml LPS for 48 h of at least three independent experiments. $*p < 0.05$. C2, C2 Cer; UT, untreated.

CD11c$^+$ cells, perhaps indicating the production of proinflammatory PAFs after LPS addition. Further analysis of PAF levels and activation of the remodeling pathway after CD and TLR stimulus will be necessary to understand the mechanisms involving PC-O in tolerance.

CE is esterified cholesterol due to the enzymatic activity of acyl CoA cholesterol acyltransferase, and is stored in lipid droplets budding from the endoplasmic reticulum (59). This process is important to reduce the level of unesterified cholesterol and for the cellular cholesterol trafficking and compartmentalization (59), however, its role in tolerance mechanisms remains to be elucidated. CE can be oxidized by lipooxigenases (60, 61) and as such can activate macrophages through TLR for the production of inflammatory reactive oxygen species and cytokines (60, 62, 63). Upon CD, but not by LPS treatment, all species of CE were upregulated in wt and *Swap70*$^{-/-}$ CD11c$^+$ cells, possibly suggesting a protolerance function of intracellular CE in contrast to their proinflammatory oxidized form.

Focusing on the inflammatory pathway and its characteristic increase in Cers, we describe SWAP-70 as a novel factor controlling Cer content and its changes in DCs. In addition to the control of total cellular Cer content, surface membrane accumulation of Cer is impaired in *Swap70*$^{-/-}$ DCs. The failure to produce normal basal levels of Cers by *Swap70*$^{-/-}$ DCs and to accumulate Cer in the plasma membrane was observed even before LPS stimulus. Activation and transport of acid sphingomyelinase from the endosomes to the plasma membrane leading to hydrolysis of SM into Cer and phosphorylcholine are the key steps required for the accumulation of Cers in DCs and macrophages in this compartment (40, 44, 49). Our study shows that activation of acid sphingomyelinase after LPS addition is impaired in *Swap70*$^{-/-}$ CD11c$^+$ cells, and this correlated with their failure to lower the endosomal pH. Thus the cells cannot establish the optimal conditions necessary for acid sphingomyelinase activity (49). Whether in the absence of SWAP-70 other mechanisms, such as lower stability, also contribute to low activity cannot be excluded. *Swap70*$^{-/-}$ CD11c$^+$ cells fail to bring acid sphingomyelinase to the cell membrane before and after LPS stimulus resulting in lower accumulation of plasma membrane Cer. The mechanism by which SWAP-70 stimulates Cer accumulation involves its control of RhoA activation as the inhibition of premature active RhoA restored the accumulation of surface Cer and promoted the localization of acid sphingomyelinase at the plasma membrane in *Swap70*$^{-/-}$ cells before and after LPS stimulus. This mechanism is similar to the regulation of the retrograde movement of MHCII in late endosomes and lysosomes to the plasma membrane of DCs by SWAP-70 (10). We propose that SWAP-70, through control of RhoA activation, regulates the vesicle trafficking necessary to translocate endosomal acid sphingomyelinase to the plasma membrane, leading to the accumulation of Cer in this compartment. Inhibition of premature RhoA activation did not, however, restore the acidification of endosomal compartments in *Swap70*$^{-/-}$ CD11c$^+$ cells after LPS stimulus (data not shown). This suggests an unknown alternative mechanism of the control of Cer generation by SWAP-70 after addition of LPS. This mechanism will be subject to future studies and it may, for example, involve the expression and/or assembly and/or regulation of the lysosomal vacuolar proton ATPase (V-H$^+$-ATPase).

GM-CSF cultures generate two CD11c$^+$ populations, a first of mature DCs and a second consisting of immature DCs, macrophage-like, and progenitor cells (4, 45–47). In this study, we demonstrated that both populations fail to accumulate surface Cer in the absence of SWAP-70. Importantly, the percentage of Cer-positive cells in both *Swap70*$^{-/-}$ populations was generally ~2 × less than the wt counterparts. In addition, similar levels of decreased surface Cer were also observed in conventional *Swap70*$^{-/-}$ DCs generated with Flt3-L in vitro. This indicates that the mechanisms leading to surface Cer accumulation regulated by SWAP-70 are the same regardless of the cell type.

A previous paper reported an increase in Cer and a reduction of SM in a mouse fetal skin-derived DC line after LPS signaling (54).

Downloaded from http://www.jimmunol.org/ by guest on February 24, 2022

In our studies using primary cell cultures, the significant increase of Cer after the LPS stimulus was not accompanied with a reduction of SM. In fact, the total sphingomyelin content remained unchanged during LPS activation in wt and *Swap70*$^{-/-}$ cells. Concentrations of SM are an order of magnitude higher than those of Cer, therefore, statistically non-significant changes in SM can result in profound changes in Cer (48). Further, the use of primary DCs instead of a cell line may explain the differences observed in the lipidomic changes between the two studies. Importantly, accumulation of Cer seems to be an important and conserved process in the lipidomics changes induced by LPS in DCs.

Cer is an important mediator of apoptosis triggered by stimuli such as radiation, TNF-α, Fas ligand, and LPS (48). Cells from mice deficient in acid sphingomyelinase (*ASMase*$^{-/-}$) accumulated less Cer and were more resistant to apoptosis after many types of stress signals (64–68). Moreover, generation of Cer by acid sphingomyelinase has been reported to be crucial in apoptosis of macrophages and DCs after LPS stimulus or upon stress conditions like serum deprivation (21, 44, 50). In line with these observations, we found significantly lower levels of apoptosis after LPS stimulus in *Swap70*$^{-/-}$ CD11c^{+} cells when compared with wt cells. Apoptosis was restored to wt levels when cell-permeable Cer was added to the cultures or by retroviral expression of SWAP-70 in *Swap70*$^{-/-}$ cells. Thus, the failure to accumulate Cer after LPS activation in the absence of SWAP-70 results in poor induction of apoptosis. Taken together, these results demonstrate a key role for SWAP-70 in the lipid dynamics such as that of Cer in DCs and macrophages and identified lipid features specific to a particular activation pathway.

Acknowledgments

We thank the members of the Jessberger and Shevchenko Laboratories for discussion and helpful advice.

Disclosures

The authors have no financial conflicts of interest.

References

1. Mellman, I. 2013. Dendritic cells: master regulators of the immune response. *Cancer Immunol. Res.* 1: 145–149.
2. Inaba, K., M. Inaba, N. Romani, H. Aya, M. Deguchi, S. Ikehara, S. Muramatsu, and R. M. Steinman. 1992. Generation of large numbers of dendritic cells from mouse bone marrow cultures supplemented with granulocyte/macrophage colony-stimulating factor. *J. Exp. Med.* 176: 1693–1702.
3. Sallusto, F., and A. Lanzavecchia. 1994. Efficient presentation of soluble antigen by cultured human dendritic cells is maintained by granulocyte/macrophage colony-stimulating factor plus interleukin 4 and downregulated by tumor necrosis factor alpha. *J. Exp. Med.* 179: 1109–1118.
4. Helft, J., J. Böttcher, P. Chakravarty, S. Zelenay, J. Huotari, B. U. Schraml, D. Goubau, and C. Reis e Sousa. 2015. GM-CSF mouse bone marrow cultures comprise a heterogeneous population of CD11c(+)MHCII(+) macrophages and dendritic cells. *Immunity* 42: 1197–1211.
5. Amit, I., M. Garber, N. Chevrier, A. P. Leite, Y. Donner, T. Eisenhaure, M. Guttman, J. K. Grenier, W. Li, O. Zuk, et al. 2009. Unbiased reconstruction of a mammalian transcriptional network mediating pathogen responses. *Science* 326: 257–263.
6. Jiang, A., O. Bloom, S. Ono, W. Cui, J. Unternaehrer, S. Jiang, J. A. Whitney, J. Connolly, J. Banchereau, and I. Mellman. 2007. Disruption of E-cadherin-mediated adhesion induces a functionally distinct pathway of dendritic cell maturation. *Immunity* 27: 610–624.
7. Manicassamy, S., B. Reizis, R. Ravindran, H. Nakaya, R. M. Salazar-Gonzalez, Y. C. Wang, and B. Pulendran. 2010. Activation of beta-catenin in dendritic cells regulates immunity versus tolerance in the intestine. *Science* 329: 849–853.
8. García-González, P., G. Ubilla-Olguín, D. Catalán, K. Schinnerling, and J. C. Aguillón. 2016. Tolerogenic dendritic cells for reprogramming of lymphocyte responses in autoimmune diseases. *Autoimmun. Rev.* 15: 1071–1080.
9. Watanabe, N., Y. H. Wang, H. K. Lee, T. Ito, Y. H. Wang, W. Cao, and Y. J. Liu. 2005. Hassall's corpuscles instruct dendritic cells to induce CD4+CD25+ regulatory T cells in human thymus. *Nature* 436: 1181–1185.
10. Ocana-Morgner, C., C. Wahren, and R. Jessberger. 2009. SWAP-70 regulates RhoA/RhoB-dependent MHCII surface localization in dendritic cells. *Blood* 113: 1474–1482.
11. Oberbanscheidt, P., S. Balkow, J. Kühnl, S. Grabbe, and M. Bähler. 2007. SWAP-70 associates transiently with macropinosomes. *Eur. J. Cell Biol.* 86: 13–24.
12. Shinohara, M., Y. Terada, A. Iwamatsu, A. Shinohara, N. Mochizuki, M. Higuchi, Y. Gotoh, S. Ihara, S. Nagata, H. Itoh, et al. 2002. SWAP-70 is a guanine-nucleotide-exchange factor that mediates signalling of membrane ruffling. *Nature* 416: 759–763.
13. Chacón-Martínez, C. A., N. Kiessling, M. Winterhoff, J. Faix, T. Müller-Reichert, and R. Jessberger. 2013. The switch-associated protein 70 (SWAP-70) bundles actin filaments and contributes to the regulation of F-actin dynamics. *J. Biol. Chem.* 288: 28687–28703.
14. Ihara, S., T. Oka, and Y. Fukui. 2006. Direct binding of SWAP-70 to non-muscle actin is required for membrane ruffling. *J. Cell Sci.* 119: 500–507.
15. Ocaña-Morgner, C., A. Götz, C. Wahren, and R. Jessberger. 2013. SWAP-70 restricts spontaneous maturation of dendritic cells. *J. Immunol.* 190: 5545–5558.
16. Ocaña-Morgner, C., P. Reichardt, M. Chopin, S. Braungart, C. Wahren, M. Gunzer, and R. Jessberger. 2011. Sphingosine 1-phosphate-induced motility and endocytosis of dendritic cells is regulated by SWAP-70 through RhoA. *J. Immunol.* 186: 5345–5355.
17. Grassmé, H., J. Riethmüller, and E. Gulbins. 2007. Biological aspects of ceramide-enriched membrane domains. *Prog. Lipid Res.* 46: 161–170.
18. Schenck, M., A. Carpinteiro, H. Grassmé, F. Lang, and E. Gulbins. 2007. Ceramide: physiological and pathophysiological aspects. *Arch. Biochem. Biophys.* 462: 171–175.
19. Zhang, Y., X. Li, K. A. Becker, and E. Gulbins. 2009. Ceramide-enriched membrane domains–structure and function. *Biochim. Biophys. Acta* 1788: 178–183.
20. Shevchenko, A., and K. Simons. 2010. Lipidomics: coming to grips with lipid diversity. *Nat. Rev. Mol. Cell Biol.* 11: 593–598.
21. Köberlin, M. S., B. Snijder, L. X. Heinz, C. L. Baumann, A. Fauster, G. I. Vladimer, A. C. Gavin, and G. Superti-Furga. 2015. A conserved circular network of coregulated lipids modulates innate immune responses. *Cell* 162: 170–183.
22. Shaikh, S. R., and M. Edidin. 2006. Polyunsaturated fatty acids, membrane organization, T cells, and antigen presentation. *Am. J. Clin. Nutr.* 84: 1277–1289.
23. Yeung, T., and S. Grinstein. 2007. Lipid signaling and the modulation of surface charge during phagocytosis. *Immunol. Rev.* 219: 17–36.
24. Shalek, A. K., R. Satija, X. Adiconis, R. S. Gertner, J. T. Gaublomme, R. Raychowdhury, S. Schwartz, N. Yosef, C. Malboeuf, D. Lu, et al. 2013. Single-cell transcriptomics reveals bimodality in expression and splicing in immune cells. *Nature* 498: 236–240.
25. Shalek, A. K., R. Satija, J. Shuga, J. J. Trombetta, D. Gennert, D. Lu, P. Chen, R. S. Gertner, J. T. Gaublomme, N. Yosef, et al. 2014. Single-cell RNA-seq reveals dynamic paracrine control of cellular variation. *Nature* 510: 363–369.
26. Van den Bossche, J., B. Malissen, A. Mantovani, P. De Baetselier, and J. A. Van Ginderachter. 2012. Regulation and function of the E-cadherin/catenin complex in cells of the monocyte-macrophage lineage and DCs. *Blood* 119: 1623–1633.
27. Vander Lugt, B., Z. T. Beck, R. C. Fuhlbrigge, N. Hacohen, J. J. Campbell, and M. Boes. 2011. TGF-β suppresses β-catenin-dependent tolerogenic activation program in dendritic cells. *PLoS One* 6: e20099.
28. Borggrefe, T., S. Keshavarzi, B. Gross, M. Wabl, and R. Jessberger. 2001. Impaired IgE response in SWAP-70-deficient mice. *Eur. J. Immunol.* 31: 2467–2475.
29. Gross, B., T. Borggrefe, M. Wabl, R. R. Sivalenka, M. Bennett, A. B. Rossi, and R. Jessberger. 2002. SWAP-70-deficient mast cells are impaired in development and IgE-mediated degranulation. *Eur. J. Immunol.* 32: 1121–1128.
30. Lutz, M. B., N. Kukutsch, A. L. Ogilvie, S. Rössner, F. Koch, N. Romani, and G. Schuler. 1999. An advanced culture method for generating large quantities of highly pure dendritic cells from mouse bone marrow. *J. Immunol. Methods* 223: 77–92.
31. Zal, T., A. Volkmann, and B. Stockinger. 1994. Mechanisms of tolerance induction in major histocompatibility complex class II-restricted T cells specific for a blood-borne self-antigen. *J. Exp. Med.* 180: 2089–2099.
32. Naik, S. H., A. I. Proietto, N. S. Wilson, A. Dakic, P. Schnorrer, M. Fuchsberger, M. H. Lahoud, M. O'Keeffe, Q. X. Shao, W. F. Chen, et al. 2005. Cutting edge: generation of splenic CD8+ and CD8- dendritic cell equivalents in Fms-like tyrosine kinase 3 ligand bone marrow cultures. *J. Immunol.* 174: 6592–6597.
33. Folch, J., M. Lees, and G. H. Sloane Stanley. 1957. A simple method for the isolation and purification of total lipides from animal tissues. *J. Biol. Chem.* 226: 497–509.
34. Schuhmann, K., R. Almeida, M. Baumert, R. Herzog, S. R. Bornstein, and A. Shevchenko. 2012. Shotgun lipidomics on a LTQ Orbitrap mass spectrometer by successive switching between acquisition polarity modes. *J. Mass Spectrom.* 47: 96–104.
35. Herzog, R., K. Schuhmann, D. Schwudke, J. L. Sampaio, S. R. Bornstein, M. Schroeder, and A. Shevchenko. 2012. LipidXplorer: a software for consensual cross-platform lipidomics. *PLoS One* 7: e29851.
36. Liebisch, G., M. Binder, R. Schifferer, T. Langmann, B. Schulz, and G. Schmitz. 2006. High throughput quantification of cholesterol and cholesteryl ester by electrospray ionization tandem mass spectrometry (ESI-MS/MS). *Biochim. Biophys. Acta* 1761: 121–128.
37. Han, X., and R. W. Gross. 2005. Shotgun lipidomics: electrospray ionization mass spectrometric analysis and quantitation of cellular lipidomes directly from crude extracts of biological samples. *Mass Spectrom. Rev.* 24: 367–412.
38. Andreyev, A. Y., E. Fahy, Z. Guan, S. Kelly, X. Li, J. G. McDonald, S. Milne, D. Myers, H. Park, A. Ryan, et al. 2010. Subcellular organelle lipidomics in TLR-4-activated macrophages. *J. Lipid Res.* 51: 2785–2797.
39. Dennis, E. A., R. A. Deems, R. Harkewicz, O. Quehenberger, H. A. Brown, S. B. Milne, D. S. Myers, C. K. Glass, G. Hardiman, D. Reichart, et al. 2010. A mouse macrophage lipidome. *J. Biol. Chem.* 285: 39976–39985.

Downloaded from http://www.jimmunol.org/ by guest on February 24, 2022

40. Avota, E., E. Gulbins, and S. Schneider-Schaulies. 2011. DC-SIGN mediated sphingomyelinase-activation and ceramide generation is essential for enhancement of viral uptake in dendritic cells. *PLoS Pathog.* 7: e1001290.
41. Perrotta, C., L. Bizzozero, D. Cazzato, S. Morlacchi, E. Assi, F. Simbari, Y. Zhang, E. Gulbins, M. T. Bassi, P. Rosa, and E. Clementi. 2010. Syntaxin 4 is required for acid sphingomyelinase activity and apoptotic function. *J. Biol. Chem.* 285: 40240–40251.
42. Rotolo, J. A., J. Zhang, M. Donepudi, H. Lee, Z. Fuks, and R. Kolesnick. 2005. Caspase-dependent and -independent activation of acid sphingomyelinase signaling. *J. Biol. Chem.* 280: 26425–26434.
43. Schneider-Brachert, W., V. Tchikov, J. Neumeyer, M. Jakob, S. Winoto-Morbach, J. Held-Feindt, M. Heinrich, O. Merkel, M. Ehrenschwender, D. Adam, et al. 2004. Compartmentalization of TNF receptor 1 signaling: internalized TNF receptosomes as death signaling vesicles. *Immunity* 21: 415–428.
44. Falcone, S., C. Perrotta, C. De Palma, A. Pisconti, C. Sciorati, A. Capobianco, P. Rovere-Querini, A. A. Manfredi, and E. Clementi. 2004. Activation of acid sphingomyelinase and its inhibition by the nitric oxide/cyclic guanosine 3′,5′-monophosphate pathway: key events in *Escherichia coli*-elicited apoptosis of dendritic cells. *J. Immunol.* 173: 4452–4463.
45. Helft, J., J. P. Böttcher, P. Chakravarty, S. Zelenay, J. Huotari, B. U. Schraml, D. Goubau, and C. Reis E Sousa. 2016. Alive but confused: heterogeneity of CD11c(+) MHC class II(+) cells in GM-CSF mouse bone marrow cultures. *Immunity* 44: 3–4.
46. Lutz, M. B., K. Inaba, G. Schuler, and N. Romani. 2016. Still alive and kicking: in-vitro-generated GM-CSF dendritic cells! *Immunity* 44: 1–2.
47. Menges, M., T. Baumeister, S. Rössner, P. Stoitzner, N. Romani, A. Gessner, and M. B. Lutz. 2005. IL-4 supports the generation of a dendritic cell subset from murine bone marrow with altered endocytosis capacity. *J. Leukoc. Biol.* 77: 535–543.
48. Hannun, Y. A., and L. M. Obeid. 2008. Principles of bioactive lipid signalling: lessons from sphingolipids. *Nat. Rev. Mol. Cell Biol.* 9: 139–150.
49. Marchesini, N., and Y. A. Hannun. 2004. Acid and neutral sphingomyelinases: roles and mechanisms of regulation. *Biochem. Cell Biol.* 82: 27–44.
50. Wang, S. W., P. Hojabrpour, P. Zhang, R. N. Kolesnick, U. P. Steinbrecher, A. Gómez-Muñoz, and V. Duronio. 2015. Regulation of ceramide generation during macrophage apoptosis by ASMase and de novo synthesis. *Biochim. Biophys. Acta* 1851: 1482–1489.
51. Mantegazza, A. R., A. Savina, M. Vermeulen, L. Pérez, J. Geffner, O. Hermine, S. D. Rosenzweig, F. Faure, and S. Amigorena. 2008. NADPH oxidase controls phagosomal pH and antigen cross-presentation in human dendritic cells. *Blood* 112: 4712–4722.
52. Haimovitz-Friedman, A., C. Cordon-Cardo, S. Bayoumy, M. Garzotto, M. McLoughlin, R. Gallily, C. K. Edwards, III, E. H. Schuchman, Z. Fuks, and R. Kolesnick. 1997. Lipopolysaccharide induces disseminated endothelial apoptosis requiring ceramide generation. *J. Exp. Med.* 186: 1831–1841.
53. Pettus, B. J., C. E. Chalfant, and Y. A. Hannun. 2002. Ceramide in apoptosis: an overview and current perspectives. *Biochim. Biophys. Acta* 1585: 114–125.
54. Santinha, D. R., D. R. Marques, E. A. Maciel, C. S. Simões, S. Rosa, B. M. Neves, B. Macedo, P. Domingues, M. T. Cruz, and M. R. Domingues. 2012. Profiling changes triggered during maturation of dendritic cells: a lipidomic approach. *Anal. Bioanal. Chem.* 403: 457–471.
55. Chabot, M. C., D. G. Greene, J. K. Brockschmidt, R. L. Capizzi, and R. L. Wykle. 1990. Ether-linked phosphoglyceride content of human leukemia cells. *Cancer Res.* 50: 7174–7178.
56. Magnusson, C. D., and G. G. Haraldsson. 2011. Ether lipids. *Chem. Phys. Lipids* 164: 315–340.
57. Morimoto, R., H. Shindou, Y. Oda, and T. Shimizu. 2010. Phosphorylation of lysophosphatidylcholine acyltransferase 2 at Ser34 enhances platelet-activating factor production in endotoxin-stimulated macrophages. *J. Biol. Chem.* 285: 29857–29862.
58. Morimoto, R., H. Shindou, M. Tarui, and T. Shimizu. 2014. Rapid production of platelet-activating factor is induced by protein kinase Cα-mediated phosphorylation of lysophosphatidylcholine acyltransferase 2 protein. *J. Biol. Chem.* 289: 15566–15576.
59. Ikonen, E. 2008. Cellular cholesterol trafficking and compartmentalization. *Nat. Rev. Mol. Cell Biol.* 9: 125–138.
60. Choi, S. H., D. Sviridov, and Y. I. Miller. 2017. Oxidized cholesteryl esters and inflammation. *Biochim. Biophys. Acta.* 1862: 393–397.
61. Hutchins, P. M., and R. C. Murphy. 2012. Cholesteryl ester acyl oxidation and remodeling in murine macrophages: formation of oxidized phosphatidylcholine. *J. Lipid Res.* 53: 1588–1597.
62. Choi, S. H., H. Yin, A. Ravandi, A. Armando, D. Dumlao, J. Kim, F. Almazan, A. M. Taylor, C. A. McNamara, S. Tsimikas, et al. 2013. Polyoxygenated cholesterol ester hydroperoxide activates TLR4 and SYK dependent signaling in macrophages. *PLoS One* 8: e83145.
63. Harkewicz, R., K. Hartvigsen, F. Almazan, E. A. Dennis, J. L. Witztum, and Y. I. Miller. 2008. Cholesteryl ester hydroperoxides are biologically active components of minimally oxidized low density lipoprotein. *J. Biol. Chem.* 283: 10241–10251.
64. Garcia-Barros, M., F. Paris, C. Cordon-Cardo, D. Lyden, S. Rafii, A. Haimovitz-Friedman, Z. Fuks, and R. Kolesnick. 2003. Tumor response to radiotherapy regulated by endothelial cell apoptosis. *Science* 300: 1155–1159.
65. Lozano, J., S. Menendez, A. Morales, D. Ehleiter, W. C. Liao, R. Wagman, A. Haimovitz-Friedman, Z. Fuks, and R. Kolesnick. 2001. Cell autonomous apoptosis defects in acid sphingomyelinase knockout fibroblasts. *J. Biol. Chem.* 276: 442–448.
66. Paris, F., H. Grassmé, A. Cremesti, J. Zager, Y. Fong, A. Haimovitz-Friedman, Z. Fuks, E. Gulbins, and R. Kolesnick. 2001. Natural ceramide reverses Fas resistance of acid sphingomyelinase($^{-/-}$) hepatocytes. *J. Biol. Chem.* 276: 8297–8305.
67. Peña, L. A., Z. Fuks, and R. N. Kolesnick. 2000. Radiation-induced apoptosis of endothelial cells in the murine central nervous system: protection by fibroblast growth factor and sphingomyelinase deficiency. *Cancer Res.* 60: 321–327.
68. Santana, P., L. A. Peña, A. Haimovitz-Friedman, S. Martin, D. Green, M. McLoughlin, C. Cordon-Cardo, E. H. Schuchman, Z. Fuks, and R. Kolesnick. 1996. Acid sphingomyelinase-deficient human lymphoblasts and mice are defective in radiation-induced apoptosis. *Cell* 86: 189–199.

Downloaded from http://www.jimmunol.org/ by guest on February 24, 2022